

Effect on 3D-printability and microstructure of pork paste partially replaced with yellow mealworm larvae paste

Jinbo Xu, Jiaqi Liu, Hui Wang, Qian Liu, Qian Chen, Fangda Sun^{*}, Baohua Kong^{*}

College of Food Science, Northeast Agricultural University, Harbin, Heilongjiang, 150030, China

ARTICLE INFO

Keywords:
Proximate composition
Microstructure
Rheological property

ABSTRACT

Yellow mealworm larvae (*Tenebrio molitor L.*) (YML) are a readily available source of non-conventional protein with high nutritional value and feed conversion efficiency. However, they remain unaccepted by most consumers. This study examines the feasibility of substituting pork paste with YML paste (YMLP) at graded substitution levels (0–75 %), while concurrently evaluating the resultant effects on both nutritional composition and 3D-printing performance parameters in pork-YML composite matrices. Proximate composition analysis showed that YML substitution elevated ash content while maintaining baseline protein levels in the composite matrices, concurrently enhancing the overall nutritional profile of the experimental samples. The mixed pastes' 3D printability was determined by measuring their rheological and microstructural properties. The Fourier-transform infrared spectroscopy results showed that the addition of YML increased the content of chitin, and the disentanglement and reorientation of chitin resulted in a decrease in viscosity and an increase in shear-thinning behavior which are shown in the rheological results. The texture profile analysis showed that the hardness, resilience, cohesiveness, and chewiness of the steamed 3D-printed samples were reduced with an increase in the YMLP replacement ratio ($P < 0.05$), which was due to the destruction of the 3D gel network as shown in scanning electron microscopy. Overall, while increasing the YMLP replacement ratio reduced the self-supporting capacity of printed samples and disrupted the 3D gel network structure, consequently diminishing printability and textural properties, successful substitution was achieved at a 30 % ratio. This optimal substitution level maintained functional performance while enhancing the nutritional profile of the pork-based matrices.

1. Introduction

In recent years, the global population has been rapidly increasing. According to statistics from the Food and Agriculture Organization of the United Nations (FAO), the world population is projected to reach 9.7 billion in 2050 (Kamalapuram et al., 2021). Meat, as a fundamental component of the human diet and a primary source of animal-derived protein, plays a critical role in global nutrition. Nevertheless, the growing global population has substantially increased the demand for animal protein, necessitating the expansion of livestock production systems. Expansion of livestock farming scale poses significant environmental challenges: excessive livestock farming not only accelerates the encroachment on arable land but also exacerbates greenhouse gas emissions from livestock rearing processes, collectively undermining ecological sustainability (Kotsou et al., 2023). Consequently, exploring novel animal-derived protein sources as sustainable alternatives to

conventional meat has become imperative.

Yellow mealworm (*Tenebrio molitor L.*) larvae (YML) are rich in proteins, fiber, vitamins, and minerals. YML's proteins are rich in leucine, isoleucine, lysine, tyrosine, and valine. Therefore, YML is recognized as an available source of non-conventional protein (Gkinali et al., 2022). Furthermore, YML's lipids are rich in monounsaturated fatty acids, which enhance YML's nutritional value. In addition, YML has a high feed conversion ratio, enabling its use in addressing food insecurity caused by overpopulation (Bordiean et al., 2020).

In recent years, several European regions have allowed edible insects, such as YML, to be used as food or food ingredients (Gkinali et al., 2022). However, a crucial issue facing the development of insect food products is that consumers currently have low acceptance. Therefore, edible insects are commonly used as food ingredients in less recognizable forms to increase consumer acceptability (Gravel and Doyen, 2020).

* Corresponding authors.

E-mail addresses: sunfangda@163.com (F. Sun), kongbh63@hotmail.com (B. Kong).

3D food printing technology is a recent food production method. Compared with traditional food processing, 3D food printing adopts an additive manufacturing technology, controlled by a computer, which stacks various ingredients layer by layer (Guo et al., 2019). Currently, 3D food printing technology is being widely researched and applied in fruit, vegetable and meat processing (Xu et al., 2023a). This is mainly because 3D food printing can produce customized food, including customized shapes, flavors, colors and nutritional content (Uribe-Alvarez et al., 2021). In addition, food production using 3D printing technology can customize foods for special populations. For example, Wang et al. (2023b) used 3D food printing technology to create an easy-to-swallow mooncake suitable for older adults with dysphagia. However, not all food materials are suitable for 3D food printing due to their rheological properties. Consequently, current research predominantly focuses on the formulation of food ink. Additionally, process parameters during printing operations also significantly determine the final print quality. For example, Ni Leam et al. (2024) studied the influence of printing parameters on sample printing effect through theory and experiment; analysis revealed that printing resolution correlates with material flow rate while exhibiting no significant association with printing velocity. Based on this mechanistic understanding, a computational framework was developed to elucidate interdependencies between key printing variables and dimensional precision. Although 3D food printing has seen steady progress, it remains in the early stages of development and further research is still needed in numerous areas. 3D printing technology is highly customizable and has broad application prospects in solving future food problems and achieving sustainable diet development. For example, Pant et al. (2022) developed spinach stems and kale stalks into food suitable for people with dysphagia using 3D food printing technology.

As a non-animal protein source with a high feed conversion rate and high nutritional value, insects are one of the key solutions to solve the food problem in the future and realize the sustainable development of diet (Derler et al., 2021; Lienhard et al., 2023; Vigneron et al., 2019). The inherent customizability of 3D food printing technology positions it as a viable processing platform for developing insect-derived food products, enabling precise control over nutritional composition and textural parameters in entomophagy applications. Several studies have reported on 3D food printing technology to make insect food products. Chao et al. (2023) used chickpea and mealworm protein isolates to 3D print a soft-textured and safe-to-swallow food for older adults. Kang et al. (2023) developed 3D-printed meat analogs with soy protein isolate and YML protein fractions. In addition, a study by Chao et al. (2022) incorporated mealworm protein isolate gel into chicken surimi using coaxial 3D printing to produce texture-modified food suitable for older adults.

Mainly YML protein has been used in developing 3D-printed foods. However, the extraction of YML protein consumes a lot of energy and requires organic reagents, such as n-hexane (Kim et al., 2020). Moreover, the extraction of YML protein will cause the loss of other nutrients. Therefore, using intact YML flour is a viable strategy to reduce production costs while maintaining nutrients. Limited literature is available on using intact YML flour as a 3D-printed food raw material; however, it has been successfully used to develop 3D-printed cereal-based food (Herdeiro et al., 2024; Severini et al., 2018). In addition, there has been limited application of whole YML, dried and ground into flour, in 3D-printed meat products, with research showing that increasing the concentration of YML negatively affected the products' flavor and color, which darkened with protein oxidation (Choi et al., 2017). Therefore, further research is needed on effectively using intact YML as a 3D-printed meat product ingredient. This study aimed to develop a highly nutritious 3D-printed food containing YML and pork and to determine the impact of YML replacement for pork on 3D printability; this included determining the effect of YML replacement on the rheological and textural properties and microstructure of the mixed pastes. This study is expected to provide useful insight into developing

3D-printed YML food products.

2. Materials and methods

2.1. Materials

In this study, 6.0 kg of fresh porcine *longissimus* muscles and 1.0 kg of back fat were purchased from Beidahuang Meat Industry Co., Ltd (Harbin, Heilongjiang, China) within 24 hours after slaughter. Freeze-dried YML was obtained from Chongyuexuan Trading Co., Ltd. (Qingdao, Shandong, China). Carrageenan (BLI1120) was obtained from the Beilian Biotechnology Co., Ltd. (Shanghai, China). Food-grade salt, mixed spices, and potato starch (Langfang Shengshijabao Food Co., Ltd., Hebei) were purchased from the RT-Mart supermarket (Harbin, China). All additives throughout this study were food-grade.

2.2. Preparation of mixed pastes

Visible connective tissue was removed from porcine *longissimus* muscles and back fat and then cut into small pieces. Pork paste was prepared by mincing 170 g of porcine *longissimus* muscles and 30 g of back fat in a meat grinder (QSJB02Y5, Bear Electric Appliance Co. Ltd., Guangdong, China) for 5 min at 4 °C.

The YML flour was prepared by crushing the freeze-dried YML for 3 min at 4 °C using a grinder (DFT-50, Dade Co., Ltd., Taizhou, Zhejiang, China). The lid was opened every minute to scrape off any adhering flour and ensure thorough grinding (particle size < 0.6 mm). The YML paste (YMLP) was prepared by mixing the YML flour and water in a grinder (QSJB02Y5, Bear Electric Appliance Co. Ltd., Guangdong, China) at a ratio of 100:173 (g/g), which is similar to the moisture content of pork paste (74.27 ± 0.06 %, based on a preliminary experiment). For the control (YM-0), the mixed spices, salt, ice water, potato starch, carrageenan, and pork paste weights were 1.5, 2.5, 70.8, 12, 1.2, and 200 g, respectively. The ingredients were mixed in a blender (SDD2001, Zhejiang Supor Limited by Share Ltd., Zhejiang, China) at 4 °C for 9 min. Subsequently, the mixed pastes were produced by replacing 15 %, 30 %, 45 %, 60 %, and 75 % of the pork paste with YMLP, labeled as YM-15, YM-30, YM-45, YM-60, and YM-75, respectively. Mixed pastes were passed through an 18-mesh sieve to eliminate residual connective tissue, then stored at 4 °C and used for 3D printing within 12 h.

2.3. Proximate composition analysis of mixed pastes

The moisture, protein, fat, and ash content of each mixed paste sample was measured according to the AOAC (2005).

2.4. Rheological properties

The rheological properties of the mixed pastes were analyzed using a rheometer (Discovery HR-1, TA Instruments Corp., New Castle, DE, USA) according to the method of Zhao et al. (2024). Two parallel plates (diameter 40 mm) were used; the gap between the parallel plates was 1 mm. The samples were placed on the bottom plate and equilibrated for 2 min at 24 °C. A layer of silicone oil covered the edges of the parallel plates to prevent moisture evaporation.

Steady shear tests were used to characterize the relationship between the pastes' viscosity and shear rate. The shear rate was between 0.01 and 10 s⁻¹ (Xu et al., 2023a). To reflect the impact of the YMLP replacement ratios on the flow behavior of the mixed pastes, fitting the viscosity-shear rate curve was achieved using the power-law model formula as follows (Xu et al., 2023a):

$$\eta = K\gamma^{n-1}$$

where η is the viscosity of mixed pastes (Pa•s), γ is the shear rate (1/s), K is the consistency index (Pa•sⁿ) and n is the flow behavior index. The

correlation coefficient (R^2) was >0.99 .

Yield stress tests were performed in oscillation stress sweep mode from 1 to 2000 Pa at 1 Hz, and the intersection point between the storage modulus (G') and loss modulus (G'') was defined as the yield stress (Wilson et al., 2017).

Frequency sweep tests were used to determine the mixed pastes' dynamic shear rheological properties. The frequency changes ranged from 0.1 to 100 Hz at 0.1 % invariant strain, which was within the linear viscoelastic region of all the samples. The changes in the G' , G'' , loss tangent ($\tan \delta$), and complex viscosity (η^*) with changes in frequency were recorded (Cao et al., 2021).

Shear recovery tests were performed in three stages as follows: (1) 180 s with a low shear rate at 1 s^{-1} , (2) rapidly increasing the shear rate from 1 to 100 s^{-1} and then holding for 120 s, and (3) rapidly dropping the shear rate from 100 to 1 s^{-1} before holding for 180. Shear recovery (%) of the mixed pastes was determined as the percentage of the average viscosity measured during the first 30 s in the third stage divided by the average viscosity acquired in the first stage (Liu et al., 2019).

2.5. Water distribution and water hold capture

The water distribution was analyzed by a low-field nuclear magnetic resonance (LF-NMR) analyzer (Bruker Optik GmbH, Ettlingen, Germany) according to the method of Zhang et al. (2021) with slight modifications. First, a mixed paste sample (approximately 2.5 g) was placed in a 15 mm diameter glass tube. The hydrogen proton signal of the sample was collected using the Carr-Purcell-Meiboom-Gill pulse sequence and the transverse relaxation time (T_2) was measured with the CONTIN algorithm. The test parameters were as follows: 0.47 T magnetic field strength, 12,000 echoes, 10 s scan interval, and 120° pulse with $200\text{ }\mu\text{s}$ interval. Each sample was scanned three times.

To determine the water holding capacity (WHC), approximately 30 g of mixed paste was placed in a polypropylene food container (Lockn Lock Co., Seoul, Korea) and sealed to isolate the water. The container was then placed in a steamer and steamed at 100°C for 15 min. Moisture contents of the steamed mixed pastes were measured according to the AOAC (2005) method. The steamed mixed pastes' WHC was measured using the method of Cao et al. (2022), with slight modifications. First, the steamed mixed pastes were cut into pieces (approximately 5 g) and weighed (w_1). Samples were wrapped in filter paper, then placed in 50 mL centrifuge tubes pre-lined with blotting paper, and centrifuged at $5000 \times g$ for 10 min at 4°C . The filter paper was removed, and the weight of the samples (w_2) was determined. The WHC was calculated using the following formula:

$$\text{WHC}(\%) = 100 \times \left(1 - \frac{w_1 - w_2}{w_1 \times w} \right)$$

where w_1 and w_2 are the weights (g) of the steamed mixed paste before and after centrifugation, respectively, and w is the moisture contents (%) of the steamed mixed paste.

2.6. Fourier-transform infrared spectroscopy

The functional groups of the mixed pastes were determined using a Vertex 70 infrared spectrometer (Bruker Optik GmbH, Ettlingen, Germany) according to the method of Zhao et al. (2024). First, the samples were vacuum-freeze dried for 48 h and ground into powder for analysis. The analysis was performed at room temperature (24°C) and the parameters for analysis were as follows: $4000\text{--}400\text{ cm}^{-1}$ scanning range, 4 cm^{-1} spectral resolution, and an average of 32 scans.

2.7. The 3D-printing process and accuracy

An extrusion-based 3D printer (FOODBOT-D1, Hangzhou Shiyin Technology Co.Ltd, Hangzhou, China) fitted with a pressure control

system was used for printing. The 3D model was designed as a cylinder with a 40 mm diameter and 20 mm height using Blender 3.3 software (Blender Foundation, Amsterdam, Netherlands; <https://www.blender.org/download/releases/3-3/>). The print parameters were set and optimized using the slicing software Slic3r (<https://slic3r.org/>) as follows: 1.35 mm layer height, 1.2 mm nozzle diameter, 80 % infill density, 25 mm/s printing speed, 24°C printing temperature and the infill pattern is rectilinear. Each mixed paste of the same batch was printed in 9 3D-printed samples and used in further measurement. The diameter and height of the print mixed pastes were measured in mm using a Vernier caliper to calculate the diameter and height accuracy, which were calculated using the following equations:

$$\text{Diameteraccuracy}(\%) = 100 \times \left(1 - \left| \frac{d_m - d_s}{d_s} \right| \right)$$

$$\text{Height accuracy}(\%) = 100 \times \left(1 - \left| \frac{h_m - h_s}{h_s} \right| \right)$$

where d_s and h_s are the set parameters for the diameter and height of the 3D model, respectively, d_m and h_m are the values for the diameter and height of the printed mixed pastes, respectively.

2.8. Texture profile analysis

The 3D-printed mixed pastes were placed in a polypropylene food container (Lockn Lock, Seoul, Korea), covered, and then placed in a steamer and steamed at 100°C for 15 min until the sample's core temperature reached 80°C . The texture profile analysis (TPA) was achieved using a TA-XT2 texture analyzer (Stable Micro Systems Ltd., Godalming, Surrey, UK) loaded with a cylindrical aluminum probe P50 (50 mm diameter) (Yu et al., 2022). The samples ($20 \times 20 \times 10\text{ mm}$) were obtained from the center of steamed 3D-printed mixed paste products. The test parameters were as follows: 5 mm/s pre-test and post-test speed, 1 mm/s test speed, 20 g trigger force, compression of 30 % of the original height, and a 5 s time interval.

2.9. Scanning electron microscopy

The samples were prepared for scanning electron microscopy (SEM) according to the method of Zhao et al. (2021), with slight modifications. First, the steamed printed samples were trimmed using a double-sided blade to $0.5 \times 0.5 \times 0.5\text{ cm}$ and fixed with glutaraldehyde in phosphate buffer (pH = 7.2) for 2 h. The samples were flushed for 1 h and eluted with an alcohol gradient. The dried samples were placed on conductive double-sided adhesive tape and coated using a Bal-Tec gold-palladium alloy coater (Leica Microsystems GmbH, Wetzlar, Germany). The acceleration voltage of the SEM (S-3400 N; Hitachi High-Tec Corp, Tokyo, Japan) was 5 kV and the magnification was $\times 1500$.

2.10. Statistical analysis

A general linear modeling procedure in the Statistix 8.1 software package (Analytical Software, Tallahassee, FL, USA) was used to analyze the data, expressed as the mean \pm standard error (SE). Significance between the means was determined by one-way analysis of variance (ANOVA) followed by Tukey's multiple comparisons test with a 95 % confidence interval ($P < 0.05$). Conducted three independent batches of experiments (replicates), and all experiments were conducted in triplicate except for the TPA, which was performed nine times. The changes in 3D printability and rheological properties of mixed pastes were described using a mixed model, the different replacement ratios were considered as fixed terms, and each replicate was considered as a random term.

Table 1

Proximate analysis of mixed pastes with different YMLP replacement levels.

Samples	Moisture (%)	Wet basis			Dry basis		
		Fat (%)	Ash (%)	Protein (%)	Fat (%)	Ash (%)	Protein (%)
YM-0	71.29 ± 0.06 ^a	11.12 ± 0.32 ^a	1.59 ± 0.03 ^d	13.90 ± 0.52 ^a	39.65 ± 1.76 ^a	5.71 ± 0.09 ^b	49.97 ± 1.88 ^a
YM-15	71.09 ± 0.38 ^a	9.75 ± 0.20 ^b	1.65 ± 0.03 ^{cd}	13.88 ± 0.25 ^a	35.17 ± 1.43 ^b	5.91 ± 0.17 ^{ab}	49.65 ± 0.48 ^a
YM-30	71.04 ± 0.22 ^a	9.14 ± 0.15 ^{bc}	1.67 ± 0.04 ^{bcd}	13.94 ± 0.37 ^a	32.12 ± 0.45 ^{bc}	5.84 ± 0.11 ^b	48.73 ± 1.02 ^a
YM-45	70.85 ± 0.12 ^a	8.77 ± 0.26 ^{cd}	1.73 ± 0.04 ^{abc}	13.96 ± 0.29 ^a	30.39 ± 0.36 ^{cd}	5.95 ± 0.13 ^{ab}	47.92 ± 0.84 ^a
YM-60	70.79 ± 0.22 ^a	8.22 ± 0.18 ^{de}	1.77 ± 0.03 ^{ab}	13.98 ± 0.29 ^a	28.42 ± 0.67 ^{cd}	6.07 ± 0.11 ^{ab}	47.88 ± 1.27 ^a
YM-75	70.63 ± 0.15 ^a	7.78 ± 0.30 ^e	1.83 ± 0.02 ^a	14.02 ± 0.36 ^a	27.33 ± 1.71 ^d	6.25 ± 0.09 ^a	47.74 ± 1.44 ^a

YM-0, YM-15, YM-30, YM-45, YM-60, and YM-75 mean that the YMLP replacement levels are 0 %, 15 %, 30 %, 45 %, 60 %, and 75 %, respectively. Values are given as means ± SE from triplicate determinations; a-e in each column represent statistically significant differences ($P < 0.05$).

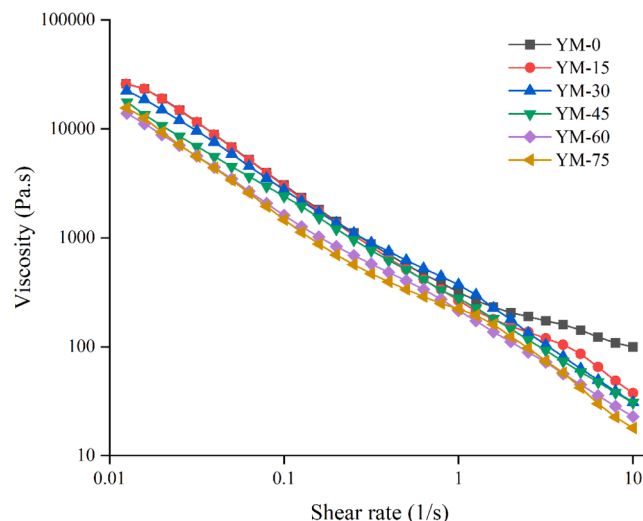


Fig. 1. Influence of different YMLP replacement levels and shear rate on viscosity of mixed pastes at room temperature (24 °C). YM-0, YM-15, YM-30, YM-45, YM-60, and YM-75 mean that the YMLP replacement levels are 0 %, 15 %, 30 %, 45 %, 60 %, and 75 %, respectively.

3. Results and discussion

3.1. Proximate composition of mixed pastes

The proximate compositions, including the moisture, protein, fat, and ash content (wet basis and dry basis) of the mixed pastes produced with different YMLP replacement ratios are shown in Table 1. The moisture of different mixed pastes was around 70 % and there was no significant difference between the pastes with different replacement ratios ($P > 0.05$). Therefore, the interference of moisture was excluded in subsequent experiments. Moreover, compared with YM-0, as the ratio of the YMLP increased from 0 % to 75 %, the mixed pastes' fat content decreased from 11.12 % to 7.78 % (wet basis) and from 39.65 % to 27.33 % (dry basis), the ash content gradually increased from 1.59 % to 1.83 % (wet basis) and from 5.71 % to 6.25 % (dry basis) ($P < 0.05$); this may be explained by the higher ash and lower fat contents of the YMLP compared with the pork paste. This finding is supported by Bordean et al. (2020), who reported that the ash content of fresh and powdered YML was higher compared with lean pork. However, there was no significant difference in protein content (wet basis and dry basis) among the mixed paste samples ($P > 0.05$); this may be due to the addition of water during the YMLP preparation, resulting in a decrease in the protein content of YMLP.

3.2. Rheological properties

The viscosity of the mixed pastes is shown in Fig. 1. All samples demonstrated shear-thinning rheological behavior, which was

Table 2

The viscosity depends on the shear rate calculated by the power-law model with different levels of YMLP replacement.

Samples	K	n
YM-0	807.25 ± 216.63	0.2450 ± 0.0649
YM-15	771.24 ± 208.37	0.2337 ± 0.0653
YM-30	621.94 ± 137.64	0.2192 ± 0.0535
YM-45	363.89 ± 47.84	0.1427 ± 0.0315
YM-60	328.88 ± 68.86	0.1839 ± 0.0504
YM-75	286.17 ± 76.47	0.1329 ± 0.0639

YM-0, YM-15, YM-30, YM-45, YM-60, and YM-75 mean that the YMLP replacement levels are 0 %, 15 %, 30 %, 45 %, 60 %, and 75 %, respectively.

confirmed by the reduction in viscosity as the shear rate increased. Specifically, when the shear rate was increased from 0.01 to 10 s⁻¹, the viscosity decreased from 22,413.20 to 99.50 Pa·s for YM-0 and 15,601.30 to 17.95 Pa·s for YM-75. During the 3D printing process, paste compositions experience varying shear rates. Typically, 3D printer nozzles have small apertures and high shear rates; therefore, pastes with a shear-thinning rheological behavior result in a low viscosity with a high shear rate at the nozzles, which is beneficial for 3D printing (Yu et al., 2023).

The power law model was used to calculate the dependence of viscosity on shear rate. The results (Table 2) show that the flow behavior index (n) of all the samples was < 1 , demonstrating the pastes' shear-thinning rheological behavior. Increasing the YMLP replacement ratio from 0 % to 75 % decreased n from 0.2450 for YM-0 to 0.1329 for YM-75. This may be due to the abundance of chitin in YML. Generally, shear thinning behavior is caused by the disentanglement of polymer chains and the redirection of needle-shaped particles. With the increasing replacement ratio of YML, the content of crystalline nanofibers and whisker-like chitin increases, which enhances the shear-thinning behavior of mixed pastes (Börzsönyi et al., 2012). The Fourier-transform infrared analysis (Fig. 6) also proves the increase in the content of chitin. In addition, the low gel strength of YML protein weakens the interaction between myofibrillar protein and can result in a shear-thinning rheological behavior (Chao et al., 2022; Demirkesen et al., 2010). The decreased n indicated the pastes' higher shear thinning behavior with an increasing YMLP ratio, which is beneficial to the 3D printing processing (Xu et al., 2023a).

The K (Pa·s^{0.5}) relates to the viscosity of a sample; a higher K indicates greater viscosity. Increasing the YMLP replacement ratio resulted in the K decreasing from 807.25 (YM-0) to 286.17 (YM-75), indicating a reduction in viscosity (Shi et al., 2022). These findings are consistent with those of Choi et al. (2017), who reported that the addition of YML protein led to a decrease in water binding ability in the sample, causing the immobilized water to convert into free water, resulting in a reduction of viscosity, this is consistent with the findings of WHC (Fig. 5D). Fig. 5C also proves that the immobilized water was converted to free water. Therefore, increasing the YMLP replacement ratio appropriately can reduce the viscosity of mixed pastes, facilitating nozzle extrusion. However, an excessively high YMLP replacement ratio may result in

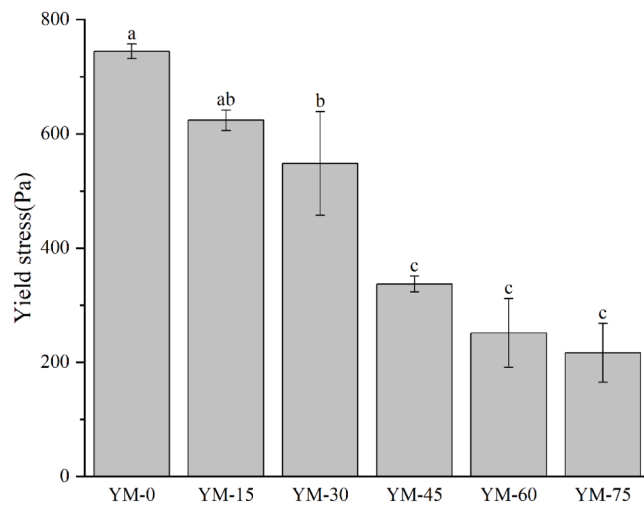


Fig. 2. Influence of YMLP replacement levels on the yield stress of mixed pastes at room temperature (24 °C). The yield stress is the intersection point of storage modulus(G') and loss modulus(G''). YM-0, YM-15, YM-30, YM-45, YM-60, and YM-75 mean that the YMLP replacement levels are 0 %, 15 %, 30 %, 30 %, 45 %, and 75 %, respectively. Yield stress with different lowercase letters(a-c) means differ significantly ($P < 0.05$). The results are mean values \pm SE ($n = 3$).

very low viscosity mixed pastes with high fluidity; this may cause poor deposition and accuracy of the 3D-printed samples (Huang et al., 2020).

The yield stress of mixed pastes is defined as the intersection point of G' and G'' (Fig. 2). A low yield stress is beneficial to extruding mixed pastes from the 3D printer nozzle (Xu et al., 2023b). The pastes' yield stress decreased significantly as the YMLP replacement ratio increased ($P < 0.05$), that is, their minimum stress to start flowing was reduced. Specifically, with an increase in the YMLP replacement ratio between 0 % and 45 %, the yield stress decreased significantly from 744.21 Pa for sample YM-0 to 336.98 Pa for sample YM-45 ($P < 0.05$). However, there was no significant difference in the yield stress when the YMLP replacement ratio exceeded 45 % ($P > 0.05$). This may be because a YMLP replacement ratio >45 % leads to the YMLP's rheological properties dominating in the mixed pastes. In addition, yield stress can reflect the ability to withstand gravity during printing. Bugarin-Castillo et al. (2023) used yield stress to calculate the maximum theoretical stable height because a higher yield stress endows lower-layer samples with the ability to resist their gravity. The results revealed that the samples with a larger yield stress printed higher heights without collapsing.

The mechanical strength and ability of samples to resist elastic deformation are represented by G' (Liu et al., 2018b). The G' and G'' values of the mixed pastes are shown in Fig. 3A and B. The G' of all the samples was higher than the G'' and both increased as the frequency increased, exhibiting a solid-like behavior of mixed pastes (Zeng et al., 2021). Specifically, when the frequency increased from 0.1 to 100 Hz, the G' increased from 4697.73 to 15,145.20 Pa for YM-0 and from 831.31 to 1982.68 Pa for YM-75 and the G'' increased from 1700.53 to 4535.59 Pa for YM-0 and from 308.50 to 1052.76 Pa for YM-75. Mixed pastes with higher G' values can exhibit better printing accuracy. However, excessively large values of G' may lead to non-continuous extrusion and a swelling phenomenon, reducing printing accuracy (Cheng et al., 2023). Moreover, with an increase in the YMLP replacement ratio, both the G' and G'' of the mixed pastes decreased. These findings are consistent with those of Kim et al. (2020), who showed that with an increasing YML protein content, the G' and G'' of meat emulsion systems decreased; this may be because low gel strength and YML protein's unstable structure lead to weak protein networks (Zhao et al., 2016). However, the research of Kang et al. (2023) showed different results. They found that adding the filtrate and pellet of YML significantly increased the G' and G'' of the samples, while adding supernatant

of YML significantly decreased both the G' and G'' . This might be attributed to the supernatant's lower gel strength and water-holding capacity. It is consistent with the findings of WHC (Fig. 5D).

The $\tan \delta$ of mixed pastes is defined as G''/G' (Fig. 3C) (Cao et al., 2022). The $\tan \delta$ of all the samples, which exhibited solid-like behavior, was <1 (Pan et al., 2022). In addition, increasing the YMLP replacement ratio caused the $\tan \delta$ to rise gradually. Specifically, as the frequency increased from 0.1 to 100 Hz, the $\tan \delta$ increased from 0.1805 to 0.2072 for the YM-0 and from 0.2755 to 0.6455 for the YM-75. These results suggest that increasing the YMLP replacement ratio reduced the solid-like behavior of the mixed pastes and enhanced their liquidity. These findings are consistent with those of Chao et al. (2022), who found that increasing mealworm protein isolate decreased the viscoelastic properties of chicken surimi ink and exhibited poor 3D printing performance. In addition, the coaxial 3D printed samples exhibited lower hardness.

Furthermore, the rheological parameters of pastes have an impact on 3D-printing performance. Outrequin et al. (2023) propose that pastes with a $\tan \delta \leq 0.268$ and $G' \geq 300$ Pa consistently result in 3D-printed samples with stable structures. As shown in Fig. 3A and C, the G' of all the samples in this study was consistently higher than 300 Pa. The YM-0 and YM-15 mixed pastes exhibited a $\tan \delta < 0.268$; however, the $\tan \delta$ of the YM-75 was consistently higher than 0.268. In contrast, the $\tan \delta$ for YM-30 was initially <0.268 but rose as the frequency was increased from 0.1 to 100 Hz. This indicates that when the replacement ratio of YMLP reaches 30 %, the samples begin to become unstable and gradually tend to become unprintable. To ensure the printed quality of 3D printed samples, the replacement ratio should be controlled at 30 % or below.

The η^* represents the extrudability of the material (Liu and Ciftci, 2021). As shown in Fig. 3D, an increasing YMLP replacement ratio reduced the η^* significantly. Specifically, as the frequency increased from 0.1 to 100 Hz, the η^* decreased from 8162.39 to 25.54 Pa·s and from 1411.24 to 3.39 Pa·s for the YM-0 and YM-75, respectively; this indicates that higher replacement ratios of YMLP make samples easier to extrude.

Three stages of shear rate were used to simulate the 3D printing process and determine changes in shear rate during printing. The viscosity changes of the mixed pastes with different YMLP replacement ratios and shear rates are presented in Fig. 4A. For the first stage, a low shear rate at 1 s^{-1} was used to simulate the flow in the print tube. The second stage, with a high shear rate at 100 s^{-1} , was used to reproduce the extrusion process from the nozzle. The third stage used a low shear rate at 1 s^{-1} to replicate the deposition process after extrusion. As shown in Fig. 4A, all the samples exhibited high viscosity in the first stage, as the YMLP replacement ratio increased, the viscosity of the samples decreased from 486.42 Pa·s for the YM-0 to 78.84 Pa·s for the YM-75. In the second stage, the viscosity decreased rapidly, and the viscosity remained below 10 Pa·s. However, in the third stage, the viscosity of all the samples recovered rapidly. Specifically, in the third stage, the viscosity of YM-0 eventually stabilized at 334.68 Pa·s, and YM-75 stabilized at 54.41 Pa·s.

The shear recovery rate of the mixed pastes is shown in Fig. 4B. The pastes' shear recovery rate with increasing YMLP replacement ratio showed a trend to initially rise and then fall; the maximum shear recovery rate was seen in YM-30. The increase in the shear recovery rate of the mixed pastes may be due to YML's lower molecular weight proteins uniformly dispersing in and filling the pores of the myofibrillar protein network, thus, enhancing the density of the network and improving the recovery rate (Kim et al., 2020; Wang et al., 2023a). However, when the YMLP's replacement ratio exceeded 45 %, the recovery rate decreased significantly ($P < 0.05$). This may be explained by the destruction of the myofibrillar protein network because of lower myofibrillar protein content, causing the recovery rate to decrease.

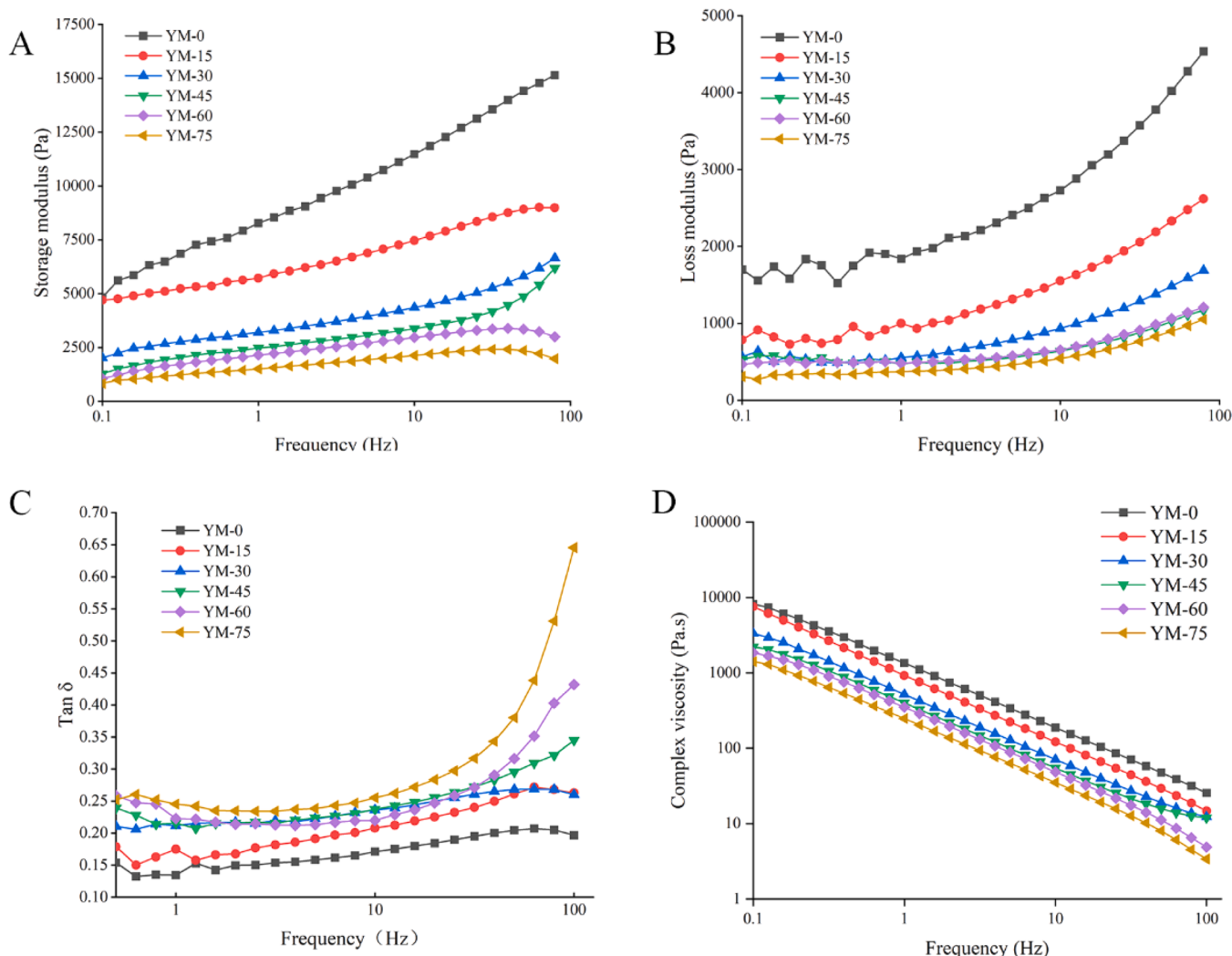


Fig. 3. A: Influence of YMLP replacement levels on storage model (G') of mixed pastes at room temperature (24 °C). B: Influence of YMLP replacement levels on loss model (G'') of mixed pastes at room temperature (24 °C). C: Influence of YMLP replacement levels on loss tangent ($\tan \delta$) of mixed pastes at room temperature (24 °C). D: Influence of YMLP replacement levels on complex viscosity (η^*) of mixed pastes at room temperature (24 °C). YM-0, YM-15, YM-30, YM-45, YM-60, and YM-75 mean that the YMLP replacement levels are 0 %, 15 %, 30 %, 45 %, 60 %, and 75 %, respectively.

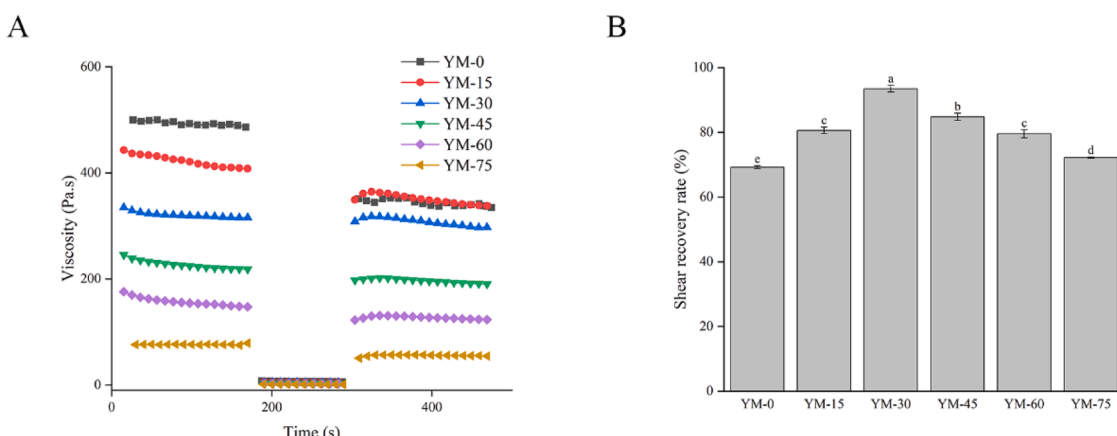


Fig. 4. A: Recovery test of mixed pastes with different YMLP replacement levels at room temperature (24 °C). The shear rate of the three stages was 1 s^{-1} (0–180 s), 100 s^{-1} (180–300 s), and 1 s^{-1} (300–480 s). B: Recovery rate of mixed pastes with different YMLP replacement levels at room temperature (24 °C). The shear recovery rate was measured by the percentage of average viscosity acquired during the first 30 s in the third stage divided by the average viscosity acquired in the first stage. YM-0, YM-15, YM-30, YM-45, YM-60, and YM-75 mean that the YMLP replacement levels are 0 %, 15 %, 30 %, 45 %, 60 %, and 75 %, respectively. Shear recovery rate with different lowercase letters (a-e) means differ significantly ($P < 0.05$). The results are mean values \pm SE ($n = 3$).

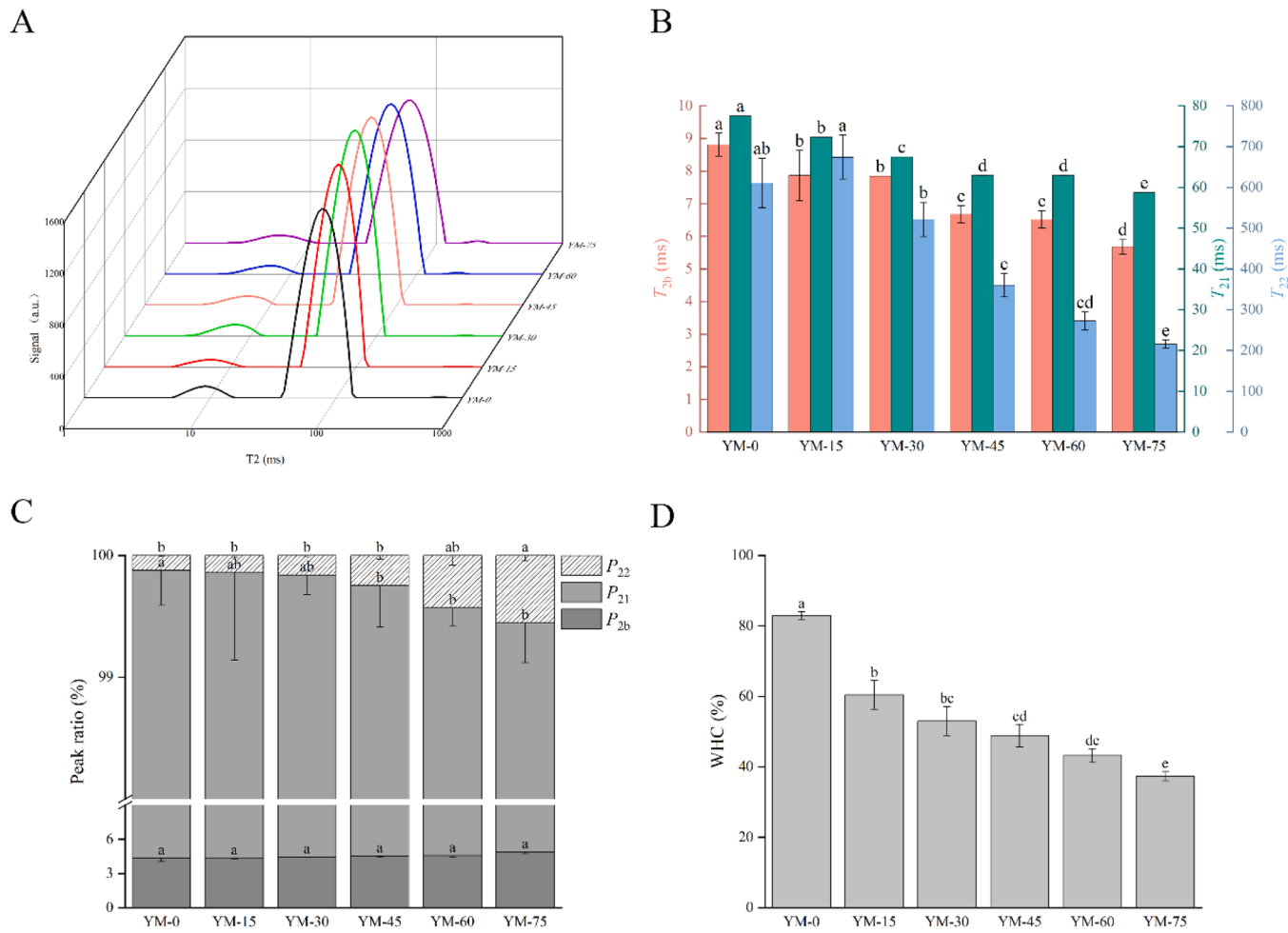


Fig. 5. A: Distribution of the LF-NMR T2 relaxation times. B: The T_{2b} , T_{21} , and T_{22} relaxation times of mixed pastes with different YMLP replacement levels. C: The P_{2b} , P_{21} , and P_{22} (the relative peak area of T_{2b} , T_{21} , and T_{22} relaxation times) of mixed pastes with different YMLP replacement levels. D: The water holds capture (WHC) of mixed pastes with different YMLP replacement levels. YM-0, YM-15, YM-30, YM-45, YM-60, and YM-75 mean that the YMLP replacement levels are 0 %, 15 %, 30 %, 45 %, 60 %, and 75 %, respectively. The T_2 , P_2 , and WHC with different lowercase letters (a-e) mean differ significantly ($P < 0.05$). The results are mean values \pm SE ($n = 3$).

3.3. Water distribution and water hold capture

To evaluate the mixed pastes' WHC and water distribution and mobility, LF-NMR was used (Xu et al., 2023b). The results are shown in Fig. 5. Three peaks are visible in Fig. 5A, corresponding to the bound water (T_{2b} at 0–10 ms), immobilized water (T_{21} at 10–100 ms) and free water (T_{22} at 100–1000 ms).

The relaxation time of the mixed pastes is presented in Fig. 5B. The shorter the relaxation time, the higher the water-binding capacity and the lower the water flow ability (Shao et al., 2016). With the increase of the YMLP replacement ratio from 0 % to 75 %, the T_{2b} , T_{21} , and T_{22} decreased from 8.81, 77.53, and 1221.55 ms, respectively, for YM-0 to 5.68, 58.73, and 430.64 ms, respectively, for YM-75. This decrease may be caused by an increase in pH (Zhang et al., 2022; Zielińska et al., 2018). Previous studies have shown that replacing the myofibrillar protein with YML protein leads to an increase in the pH of emulsion systems. This phenomenon is principally attributed to the comparatively elevated pH value of YML protein relative to myofibrillar protein (Choi et al., 2017; Kim et al., 2020). At a pH range of 5 – 9, the solubility of YML proteins rapidly increases as the pH increases, enhancing the water-binding capacity of mixed pastes (Zielińska et al., 2018). In addition, due to deviation from the protein isoelectric point, solubility of myofibrillar protein will also increase, which is also beneficial for reducing the relaxation time and moisture fluidity of the sample (Sun

et al., 2020).

P_{2b} , P_{21} , and P_{22} correspond to the relative contents of bound, immobilized, and free water. As shown in Fig. 5C, the P_{2b} of all the samples with different YMLP replacement ratios between 0 % and 75 % were not significantly different ($P > 0.05$). The increase of the YMLP replacement ratio significantly decreased the P_{21} from 95.42 % for YM-0 to 91.97 % for YM-75. In contrast, there was an increase in the P_{22} from 0.12 % for YM-0 to 0.54 % for YM-75; this finding indicates that part of the immobilized water was converted to free water ($P < 0.05$). This may be due to the more stable structure of the myofibrillar proteins compared with the YML proteins' structure, which endows the myofibrillar protein with a stronger ability to trap water molecules (Choi et al., 2011; Kim et al., 2020). The increase in the YMLP replacement ratio causes a decrease in myofibrillar protein content, which reduces the ability to trap water molecules and leads to the transfer of immobilized water to free water. However, as shown in Fig. 5B, while the immobilized water was converted into free water, the T_{2b} , T_{21} , and T_{22} decreased simultaneously, resulting in higher water-binding capacity. This may be due to an increase in the content of chitin, which is abundant in YML, at a higher replacement ratio, resulting in poorer water retention (Zhang et al., 2022). Although the water-binding ability of the individual protein molecules rises, the ratio of hydrophobic substances also increases, increasing the pastes' water-binding capacity, while transferring immobilized water to free water.

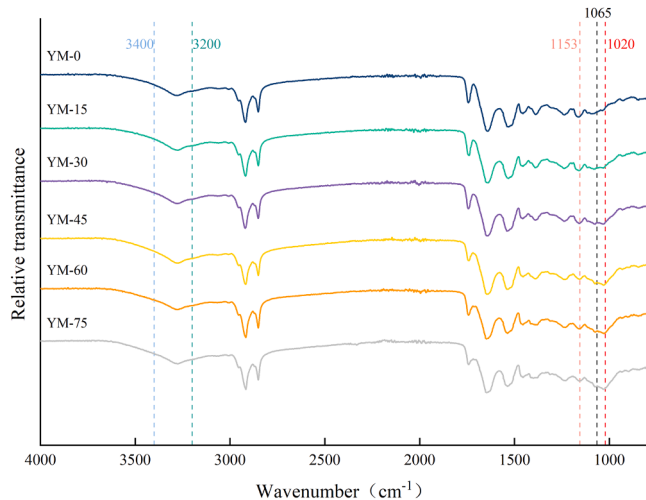


Fig. 6. FT-IR spectra of mixed pastes with different YMLP replacement levels. YM-0, YM-15, YM-30, YM-45, YM-60, and YM-75 mean that the YMLP replacement levels are 0 %, 15 %, 30 %, 45 %, 60 %, and 75 %, respectively.

The WHC is an important property of meat products and influences their color and texture profile (Hughes et al., 2014). As shown in Fig. 5D, with an increase in the YMLP replacement ratio, the WHC reduced significantly from 82.94 % for YM-0 to 37.34 % for YM-75 ($P < 0.05$). These results are consistent with those of Kim et al. (2020), who found that increasing the *T. molitor* protein concentration in meat emulsions significantly reduced their WHC ($P < 0.05$). This phenomenon may be because the myofibrillar protein forms a better gel network structure

after heating compared with the YML proteins (Khampakool et al., 2020).

3.4. Fourier-transform infrared analysis

Fourier-transform infrared spectroscopy was used to detect the hydrogen bonds and functional groups in the mixed pastes. Bands around 1065 cm⁻¹ and 1153 cm⁻¹ are N-acetylglucosamine rings and oxygen connecting two N-acetylglucosamine rings, respectively, which are characteristic of chitin (Kabalak et al., 2020). In addition, an absorption band at 1010–1030 cm⁻¹ indicates C—O—C stretching vibrations in chitosan molecules (Cheraghi et al., 2022). As shown in Fig. 6, with an increase in the YMLP replacement ratio, the absorption peak at 1010–1030 cm⁻¹ gradually increased, indicating an increased chitin content. This result was anticipated as YML contains abundant chitin, which is rich in the hydroxyl groups that facilitate the formation of hydrogen bonds (Adamkova et al., 2017; Lv et al., 2023). In addition, all samples showed spectral broadbands between 3200 and 3400 cm⁻¹, indicating the vibrational stretching of free, inter-, and intra-molecularly bound hydroxyl groups (Zhao et al., 2024). Moreover, with an increase in the YMLP replacement ratio, the wave number of the peak position shifted from 3283 cm⁻¹ (YM-0) to 3275 cm⁻¹ (YM-75), indicating the formation of stronger hydrogen bonds and hydrogen bonding (Nagasaki et al., 2021). Additionally, samples from YM-0 to YM-30, which exhibited higher strength intermolecular forces, had higher recovery rates. However, as the YMLP replacement ratio increased, the myofibrillar protein network was destroyed, and the hydrogen bonds were no longer sufficient to support the recovery of the mixed pastes after a high shear rate. This causing the recovery rate to decrease as the replacement ratio of YMLP was increased from 0 % to 45 %.

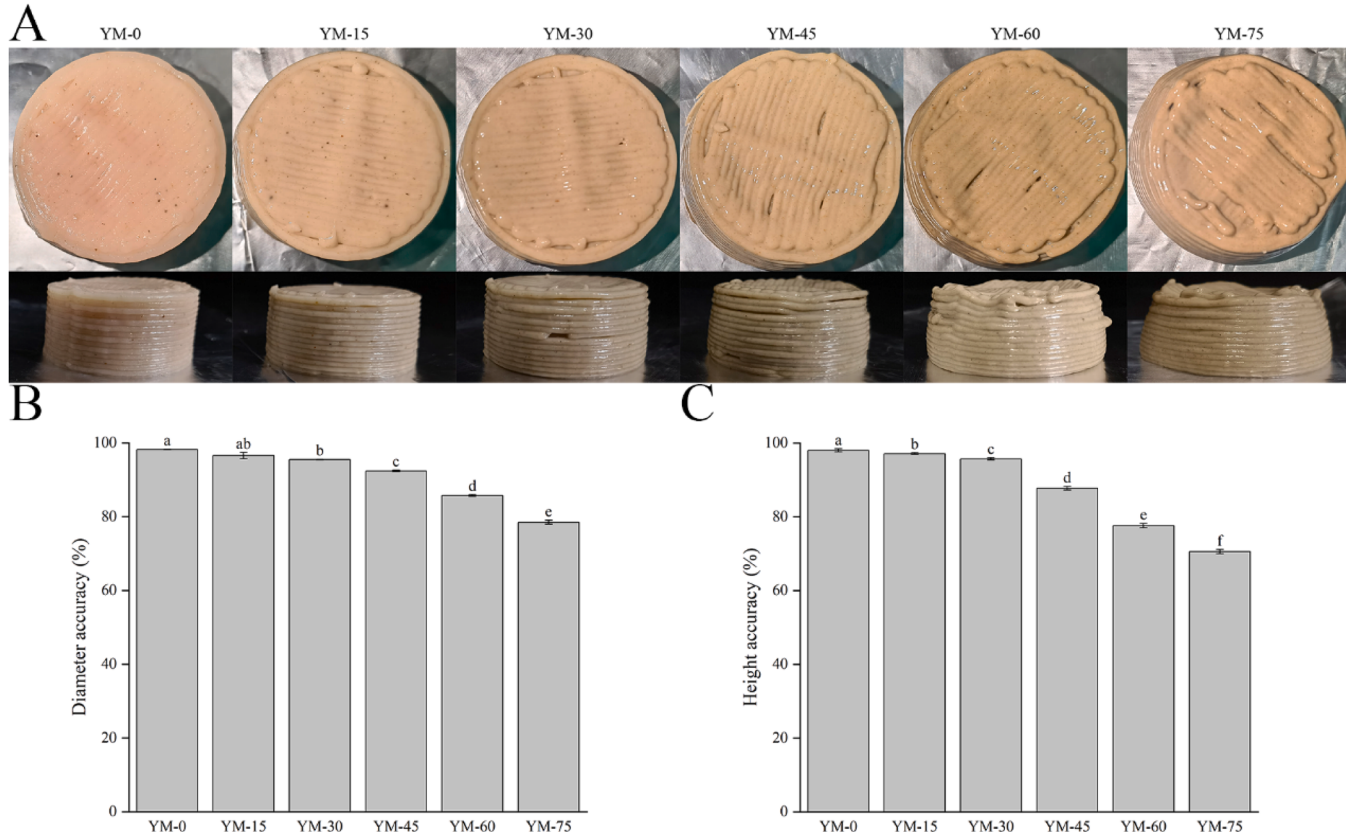


Fig. 7. The images (A), diameter accuracy (B), and height accuracy (C) of 3D-printed mixed pastes with different YMLP replacement levels. YM-0, YM-15, YM-30, YM-45, YM-60, and YM-75 mean that the YMLP replacement levels are 0 %, 15 %, 30 %, 45 %, 60 %, and 75 %, respectively. Diameter accuracy and height accuracy with different lowercase letters (a-f) means differ significantly ($P < 0.05$). The results are mean values \pm SE ($n = 3$).

Table 3
Textural properties of steamed 3D printed mixed pastes.

Samples	Hardness (N)	Resilience	Springiness	Cohesiveness	Chewiness (N)
YM-0	17.71 ± 0.50 ^a	0.39 ± 0.03 ^a	0.91 ± 0.05 ^b	0.75 ± 0.02 ^a	12.02 ± 0.42 ^a
YM-15	15.31 ± 0.38 ^b	0.37 ± 0.04 ^b	0.90 ± 0.04 ^b	0.73 ± 0.03 ^b	10.12 ± 0.27 ^b
YM-30	13.05 ± 0.37 ^c	0.36 ± 0.04 ^c	0.90 ± 0.05 ^b	0.73 ± 0.04 ^{abc}	8.63 ± 0.31 ^c
YM-45	11.22 ± 0.14 ^d	0.35 ± 0.03 ^d	0.90 ± 0.04 ^b	0.73 ± 0.02 ^{cd}	7.34 ± 0.16 ^d
YM-60	9.86 ± 0.33 ^e	0.34 ± 0.03 ^e	0.90 ± 0.06 ^b	0.72 ± 0.03 ^d	6.32 ± 0.23 ^e
YM-75	6.56 ± 0.37 ^f	0.29 ± 0.04 ^f	0.93 ± 0.07 ^a	0.68 ± 0.04 ^e	4.12 ± 0.31 ^f

YM-0, YM-15, YM-30, YM-45, YM-60, and YM-75 mean that the YMLP replacement levels are 0 %, 15 %, 30 %, 45 %, 60 %, and 75 %, respectively. Values are given as means ± SE ($n = 9$); a-f in each column represent statistically significant differences ($P < 0.05$).

3.5. The accuracy of 3D-printed mixed pastes

The accuracy of 3D printing relates to how closely the product's design specifications are met and is an important indicator for assessing the effectiveness of the processing. The effect of different YMLP replacement ratios on the mixed pastes' 3D images and printing accuracy is presented in Fig. 7A, B, and C. The control with a YMLP replacement ratio of 0 % had the best 3D printing effect and the highest diameter and height accuracy. As the YMLP replacement ratio increased, the diameter and height accuracy reduced significantly ($P < 0.05$), which is consistent with the results for the G' (Fig. 3A) and yield stress (Fig. 2). A reduction of the G' and yield stress reduces the pastes' self-supporting ability. Poor self-supporting ability makes it impossible for the bottom layer of the printing mixed pastes to support the gravity generated by sample accumulation during the printing process, which may cause the collapse of the samples (Liu et al., 2018a). Specifically, when the YMLP replacement ratio exceeded 30 %, the samples collapsed substantially with the twisting and interruption of 3D-printed lines; in addition, the accuracy of the diameter and height decreased rapidly. This finding is consistent with the shear recovery rate results (Fig. 4B). When the YMLP replacement ratio exceeded 30 %, the mixed pastes'

recovery rate reduced rapidly, and they were unable to restore viscosity to the pre-extrusion state after extrusion; in addition, a significant decrease in the resolution and accuracy of printing was observed.

3.6. Texture profile analysis

The steamed 3D-printed mixed pastes' textural properties were determined by TPA. As shown in Table 3, the hardness, resilience, cohesiveness, and chewiness reduced with an increase in YMLP replacement ratio from 17.71 N, 0.39, 0.75, and 12.02 N for YM-75 ($P < 0.05$). These results are consistent with the findings of Zhang et al. (2022), who found that the textural properties of frankfurters decreased as the replacement ratio of pre-dried mealworm larvae flour increased. However, an increase in YMLP replacement ratios has no significant effect on mixed pastes' springiness. The decrease in textural properties may be a result of the destruction of the 3D gel network (Liu et al., 2015). The water distribution and WHC significantly influence the textural properties of samples. Wu et al. (2022) consider that disruption of protein-water interactions induces elevated free water content and concomitant WHC reduction. During thermal processing, the water loss caused by the decrease in WHC can damage the microstructure of the sample and lead to a deterioration of texture properties (Wu et al., 2022).

3.7. Microstructures

The microstructures of the 3D print mixed pastes are shown in Fig. 8. The control (YM-0) had the densest network structure. As the YMLP replacement ratio increased, the mixed pastes' 3D gel network structure was destroyed and the diameter of the mesh gradually increased. This is consistent with the results of the TPA (Table 3). Myofibrillar protein can form thermally irreversible links and induce the elasticity and toughness of samples after heat treatment (Liu et al., 2011). However, YML proteins are low molecular weight non-muscle proteins; replacing pork with YMLP reduces the content of myofibrillar protein in the mixed pastes and therefore, obstructs the formation of a 3D gel network (Kim et al., 2021). In addition, YML proteins have a certain hydrophilicity and active charges, which cause the partial unfolding of the myofibrillar proteins' conformation and decrease their aggregation and compatibility (Kim et al., 2021; Yi et al., 2013). The SEM results confirmed that

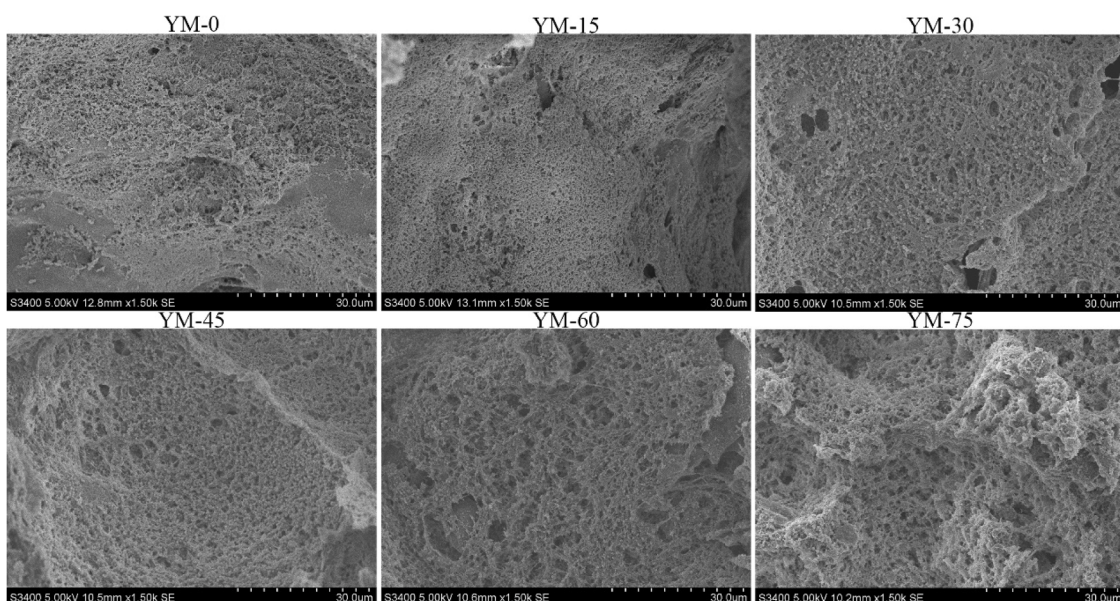


Fig. 8. Micrographs (magnification $\times 1500$) of steamed 3D printed mixed pastes. YM-0, YM-15, YM-30, YM-45, YM-60, and YM-75 mean that the YMLP replacement levels are 0 %, 15 %, 30 %, 45 %, 60 %, and 75 %, respectively.

the YML proteins did not participate in the formation of the 3D gel network. Moreover, with an increasing YMLP replacement ratio, the pastes' 3D gel network structures were destroyed, leading to a reduction of the mixed pastes' textural properties and WHC.

4. Conclusions

This study aimed to replace pork paste with different ratios of YMLP to develop a highly nutritional 3D-printed food. Compared with YM-0, including YMLP increased the ash content and decreased the fat content of the 3D-printed food, thereby increasing the nutritional value. However, the study results showed that the viscosity, G' , G'' , and η^* decreased significantly with an increase in the YMLP replacement ratio. Therefore, the replacement of pork paste with YMLP reduced the mixed pastes' self-supporting properties, thereby resulting in poor 3D printing performance and reduced accuracy. Our results indicated that 30 % was the maximum YMLP replacement ratio for an acceptable mixed paste product appearance. In addition, the replacement of pork paste with YMLP destroyed the 3D gel network structure of the steamed printed samples in a ratio-dependent manner, leading to a reduction of WHC and poorer textural properties. Therefore, further research will focus on improving the textural properties and flavor of 3D-printed YML food.

Ethical statement

This article does not contain any studies with animals and human performed by any of the authors.

CRediT authorship contribution statement

Jinbo Xu: Writing – original draft, Methodology, Investigation, Formal analysis, Data curation. **Jiaqi Liu:** Investigation, Data curation. **Hui Wang:** Validation, Software. **Qian Liu:** Visualization, Validation, Supervision. **Qian Chen:** Methodology, Investigation, Funding acquisition. **Fangda Sun:** Software, Resources, Project administration. **Baohua Kong:** Writing – review & editing, Funding acquisition.

Declaration of competing interest

The authors declare that they have no known competing financial interests or personal relationships that could have appeared to influence the work reported in this paper.

Acknowledgments

This study was funded by the National Key Research and Development Program during the 14th Five-year in China (2023YFD2100102) and the Major Science and Technology Projects in Heilongjiang province (2021ZX12B05).

Data availability

Data will be made available on request.

References

- Adamkova, A., Mlcek, J., Kourimska, L., Borkovcova, M., Busina, T., Adamek, M., Bednarova, M., Krajsa, J., 2017. Nutritional potential of selected insect species reared on the Island of sumatra. *Int. J. Env. Res. Public Health* 14 (5). <https://doi.org/10.3390/ijerph14050521>.
- AOAC, C., 2005. *Official Methods of Analysis of the Association of Analytical Chemists International. Official Methods*, Gaithersburg, MD, USA.
- Bordjean, A., Krzyżaniak, M., Stolarski, M.J., Czachorowski, S., Peni, D., 2020. Will yellow mealworm become a source of safe proteins for Europe? *Agriculture* 10 (6). <https://doi.org/10.3390/agriculture10060233>.
- Börzsönyi, T., Szabó, B., Törös, G., Wegner, S., Török, J., Somfai, E., Bien, T., Stannarius, R., 2012. Orientational order and alignment of elongated particles induced by shear. *Phys. Rev. Lett.* 108 (22), 228302. <https://doi.org/10.1103/physrevlett.108.228302>.
- Bugarin-Castillo, Y., Rando, P., Clabaux, M., Moulin, G., Ramaioli, M., 2023. 3D printing to modulate the texture of starch-based food. *J. Food Eng.* 350. <https://doi.org/10.1016/j.jfoodeng.2023.111499>.
- Cao, C., Feng, Y., Kong, B., Xia, X., Liu, M., Chen, J., Zhang, F., Liu, Q., 2021. Textural and gel properties of frankfurters as influenced by various kappa-carrageenan incorporation methods. *Meat. Sci.* 176, 108483. <https://doi.org/10.1016/j.meatsci.2021.108483>.
- Cao, F., Chen, R., Li, Y., Han, R., Li, F., Shi, H., Jiao, Y., 2022. Effects of NaCl and MTGase on printability and gelling properties of extrusion-based 3D printed white croaker (*Argyrosomus argentatus*) surimi. *LWT* 164. <https://doi.org/10.1016/j.lwt.2022.113646>.
- Chao, C., Hwang, J.S., Kim, I.W., Choi, R.Y., Kim, H.W., Park, H.J., 2022. Coaxial 3D printing of chicken surimi incorporated with mealworm protein isolate as texture-modified food for the elderly. *J. Food Eng.* 333. <https://doi.org/10.1016/j.jfoodeng.2022.111151>.
- Chao, C., Lee, J.H., Kim, I.W., Choi, R.Y., Kim, H.W., Park, H.J., 2023. Investigation of 3D-printable chickpea-mealworm protein mixtures and their bolus rheology: a soft-textured and safe-swallowing food for the elderly. *Food Biosci.* 54. <https://doi.org/10.1016/j.fbio.2023.102924>.
- Cheng, Y., Liang, K., Chen, Y., Gao, W., Kang, X., Li, T., Cui, B., 2023. Effect of molecular structure changes during starch gelatinization on its rheological and 3D printing properties. *Food Hydrocoll.* 137. <https://doi.org/10.1016/j.foodhyd.2022.108364>.
- Cheraghi, E., Kababian, M., Moradi-Asl, E., Bafrouyi, S.M.M., Saghafipour, A., 2022. Structure and antibacterial activity of Chitosan from the American cockroach, the German cockroach and the mealworm beetle. *J. Arthropod. Borne Dis.* 16 (4), 325.
- Choi, Y.-S., Park, K.-S., Kim, H.-Y., Kim, H.-W., Song, D.-H., Chung, H.-J., Lee, J.-W., Kim, C.-J., 2011. Interactions between chicken salt-soluble meat proteins and Makgeolli Lees Fiber in heat-induced gels. *Korean J. Food Sci. Anim. Resour.* 31 (6), 817–826. <https://doi.org/10.5851/kosfa.2011.31.6.817>.
- Choi, Y.S., Kim, T.K., Choi, H.D., Park, J.D., Sung, J.M., Jeon, K.H., Paik, H.D., Kim, Y.B., 2017. Optimization of replacing pork meat with yellow worm (*Tenebrio molitor* L.) for frankfurters. *Korean J. Food Sci. Anim. Resour.* 37 (5), 617–625. <https://doi.org/10.5851/kosfa.2017.37.5.617>.
- Demirkesen, I., Mert, B., Sumru, G., Sahin, S., 2010. Rheological properties of gluten-free bread formulations. *J. Food Eng.* 96 (2), 295–303. <https://doi.org/10.1016/j.jfoodeng.2009.08.004>.
- Derler, H., Lienhard, A., Berner, S., Grasser, M., Posch, A., Rehorska, R., 2021. Use them for what they are good at: mealworms in circular food systems. *Insects* 12 (1). <https://doi.org/10.3390/insects12010040>.
- Gkinali, A.-A., Matsakidou, A., Vasileiou, E., Paraskevopoulou, A., 2022. Potentiality of *tenebrio molitor* larva-based ingredients for the food industry: a review. *Trends. Food Sci. Technol.* 119, 495–507. <https://doi.org/10.1016/j.tifs.2021.11.024>.
- Gravel, A., Doyen, A., 2020. The use of edible insect proteins in food: challenges and issues related to their functional properties. *Innov. Food Sci. Emerg. Technol.* 59, 102272. <https://doi.org/10.1016/j.ifset.2019.102272>.
- Guo, C., Zhang, M., Bhandari, B., 2019. Model building and slicing in food 3D printing processes: a review. *Compr. Rev. Food Sci. Food Saf.* 18 (4), 1052–1069. <https://doi.org/10.1111/1541-4337.12443>.
- Herdeiro, F.M., Carvalho, M.O., Nunes, M.C., Raymundo, A., 2024. Development of healthy snacks incorporating meal from *Tenebrio molitor* and *Alphitobius diaperinus* using 3D printing technology. *Foods* 13 (2). <https://doi.org/10.3390/foods13020179>.
- Huang, M.s., Zhang, M., Guo, C.f., 2020. 3D printability of brown rice gel modified by some food hydrocolloids. *J. Food Process. Preserv.* 44 (7). <https://doi.org/10.1111/jfpp.14502>.
- Hughes, J.M., Oiseth, S.K., Purslow, P.P., Warner, R.D., 2014. A structural approach to understanding the interactions between colour, water-holding capacity and tenderness. *Meat. Sci.* 98 (3), 520–532. <https://doi.org/10.1016/j.meatsci.2014.05.022>.
- Kabalak, M., Aracagok, D., Torun, M., 2020. Extraction, characterization and comparison of chitins from large bodied four Coleoptera and orthoptera species. *Int. J. Biol. Macromol.* 145, 402–409. <https://doi.org/10.1016/j.ijbiomac.2019.12.194>.
- Kamalapuram, S.K., Handral, H., Choudhury, D., 2021. Cultured meat prospects for a billion! *Foods* 10 (12). <https://doi.org/10.3390/foods10122922>.
- Kang, T.W., Choi, R.-Y., Kim, I.-W., Lee, E.-J., Kim, H.W., Park, H.J., 2023. Evaluation of feasibility of *tenebrio molitor* larval fractions as a meat analog using 3D printing. *Innov. Food Sci. Emerg. Technol.* 89. <https://doi.org/10.1016/j.ifset.2023.103446>.
- Khampakool, A., Soisungwan, S., You, S., Park, S.H., 2020. Infrared assisted freeze-drying (IRAFD) to produce shelf-stable insect food from protaetia brevitarsis (White-Spotted Flower Chafer) larva. *Food Sci. Anim. Resour.* 40 (5), 813–830. <https://doi.org/10.5851/kosfa.2020.e60>.
- Kim, T.K., Lee, M.H., Yong, H.I., Jung, S., Paik, H.D., Jang, H.W., Choi, Y.S., 2020. Effect of interaction between mealworm protein and myofibrillar protein on the rheological properties and thermal stability of the prepared emulsion systems. *Foods* 9 (10). <https://doi.org/10.3390/foods9101443>.
- Kim, T.K., Yong, H.I., Sung, J.M., Jang, H.W., Choi, Y.S., 2021. Effect of conjugated protein composed of porcine myofibril and protaetia brevitarsis protein on protein functionality. *J. Insects Food Feed* 7 (7), 1101–1110. <https://doi.org/10.3920/jiff2020.0159>.
- Kotsou, K., Chatzimilitakos, T., Athanasiadis, V., Bozinou, E., Athanassiou, C.G., Lalas, S.I., 2023. Innovative applications of *Tenebrio molitor* Larvae in food product development: a comprehensive review. *Foods* 12 (23). <https://doi.org/10.3390/foods12234223>.
- Lienhard, A., Rehorska, R., Pollinger-Zierler, B., Mayer, C., Grasser, M., Berner, S., 2023. Future proteins: sustainable diets for *Tenebrio molitor* rearing composed of food by-products. *Foods* 12 (22). <https://doi.org/10.3390/foods12224092>.

- Liu, L., Ciftci, O.N., 2021. Effects of high oil compositions and printing parameters on food paste properties and printability with a 3D printing food processing model. *J. Food Eng.* 288. <https://doi.org/10.1016/j.jfoodeng.2020.110135>.
- Liu, R., Zhao, S.-M., Xie, B.-J., Xiong, S.-B., 2011. Contribution of protein conformation and intermolecular bonds to fish and pork gelation properties. *Food Hydrocoll.* 25 (5), 898–906. <https://doi.org/10.1016/j.foodhyd.2010.08.016>.
- Liu, S., Chan, W.L., Li, L., 2015. Rheological properties and scaling laws of κ-carrageenan in aqueous solution. *Macromolecules* 48 (20), 7649–7657. <https://doi.org/10.1021/acs.macromol.5b01922>.
- Liu, Z., Bhandari, B., Prakash, S., Mantihal, S., Zhang, M., 2019. Linking rheology and printability of a multicomponent gel system of carrageenan-xanthan-starch in extrusion-based additive manufacturing. *Food Hydrocoll.* 87, 413–424. <https://doi.org/10.1016/j.foodhyd.2018.08.026>.
- Liu, Z., Zhang, M., Bhandari, B., 2018a. Effect of gums on the rheological, microstructural and extrusion printing characteristics of mashed potatoes. *Int. J. Biol. Macromol.* 117, 1179–1187. <https://doi.org/10.1016/j.ijbiomac.2018.06.048>.
- Liu, Z., Zhang, M., Yang, C.-h., 2018b. Dual extrusion 3D printing of mashed potatoes/strawberry juice gel. *LWT* 96, 589–596. <https://doi.org/10.1016/j.lwt.2018.06.014>.
- Lv, J., Lv, X., Ma, M., Oh, D.H., Jiang, Z., Fu, X., 2023. Chitin and chitin-based biomaterials: a review of advances in processing and food applications. *Carbohydr. Polym.* 299, 120142. <https://doi.org/10.1016/j.carbpol.2022.120142>.
- Nagasaki, A., Matsuba, G., Ikemoto, Y., Moriwaki, T., Ohta, N., Osaka, K., 2021. Analysis of the sol and gel structures of potato starch over a wide spatial scale. *Food Sci. Nutr.* 9 (9), 4916–4926. <https://doi.org/10.1002/fsn3.2441>.
- Ni Leam, P.X., Pant, A., An, J., Huei Leo, C., Tan, U.X., Kai Chua, C., 2024. A preliminary investigation on the effect of ingredient flow speed in extrusion-based printing through experimental and theoretical approaches. *Int. J. Bioprinting* 0 (0). <https://doi.org/10.36922/ijb.2787>.
- Outrequin, T.C.R., Gamonpilas, C., Siriwatwechakul, W., Sreearunothai, P., 2023. Extrusion-based 3D printing of food biopolymers: a highlight on the important rheological parameters to reach printability. *J. Food Eng.* 342. <https://doi.org/10.1016/j.jfoodeng.2022.111371>.
- Pan, H., Pei, F., Ma, G., Ma, N., Zhong, L., Zhao, L., Hu, Q., 2022. 3D printing properties of *Flammulina velutipes* polysaccharide-soy protein complex hydrogels. *J. Food Eng.* 334. <https://doi.org/10.1016/j.jfoodeng.2022.111170>.
- Pant, A., Ni Leam, P.X., Chua, C.K., Tan, U.X., 2022. Valorisation of vegetable food waste utilising three-dimensional food printing. *Virtual Phys. Prototyp.* 18 (1). <https://doi.org/10.1080/17452759.2022.2146593>.
- Severini, C., Azzolini, D., Albenzio, M., Derossi, A., 2018. On printability, quality and nutritional properties of 3D printed cereal based snacks enriched with edible insects. *Food Res. Int.* 106, 666–676. <https://doi.org/10.1016/j.foodres.2018.01.034>.
- Shao, J.-H., Deng, Y.-M., Song, L., Batur, A., Jia, N., Liu, D.-Y., 2016. Investigation the effects of protein hydration states on the mobility water and fat in meat batters by LF-NMR technique. *LWT - Food Sci. Technol.* 66, 1–6. <https://doi.org/10.1016/j.lwt.2015.10.008>.
- Shi, Y., Zhang, M., Phuhongsung, P., 2022. Microwave-induced spontaneous deformation of purple potato puree and oleogel in 4D printing. *J. Food Eng.* 313. <https://doi.org/10.1016/j.jfoodeng.2021.110757>.
- Sun, Q., Zhang, C., Li, Q., Xia, X., Kong, B., 2020. Changes in functional properties of common carp (Cyprinus carpio) myofibrillar protein as affected by ultrasound-assisted freezing. *J. Food Sci.* 85 (9), 2879–2888. <https://doi.org/10.1111/1750-3841.15386>.
- Uribe-Alvarez, R., O'Shea, N., Murphy, C.P., Coleman-Vaughan, C., Guinee, T.P., 2021. Evaluation of rennet-induced gelation under different conditions as a potential method for 3D food printing of dairy-based high-protein formulations. *Food Hydrocoll.* 114. <https://doi.org/10.1016/j.foodhyd.2020.106542>.
- Vigneron, A., Jehan, C., Rigaud, T., Moret, Y., 2019. Immune defenses of a beneficial pest: the mealworm beetle, *tenebrio molitor*. *Front. Physiol.* 10, 138. <https://doi.org/10.3389/fphys.2019.00138>.
- Wang, M., Zhao, Y., Wang, M., Zhang, Z., Huang, M., Wang, K., Shao, J., Sun, J., 2023a. Effects of *tenebrio molitor* protein emulsion on the properties and structure of myofibrillar protein gel. *LWT* 189. <https://doi.org/10.1016/j.lwt.2023.115511>.
- Wang, X., Zhang, M., Mujumdar, A.S., Li, J., 2023b. Easy-to-swallow mooncake using 3D printing: effect of oil and hydrocolloid addition. *Food Res. Int.* 164, 112404. <https://doi.org/10.1016/j.foodres.2022.112404>.
- Wilson, S.A., Cross, L.M., Peak, C.W., Gaharwar, A.K., 2017. Shear-thinning and thermo-reversible nanoengineered inks for 3D bioprinting. *ACS Appl. Mater. Interfaces* 9 (50), 43449–43458. <https://doi.org/10.1021/acsami.7b13602>.
- Wu, Z., Ma, W., Xue, S.J., Zhou, A., Liu, Q., Hui, A., Shen, Y., Zhang, W., Shi, J., 2022. Ultrasound-assisted immersion thawing of prepared ground pork: effects on thawing time, product quality, water distribution and microstructure. *LWT* 163. <https://doi.org/10.1016/j.lwt.2022.113599>.
- Xu, J., Fan, Y., Chen, Q., Sun, F., Li, M., Kong, B., Xia, X., 2023a. Effects of kappa-carrageenan gum on 3D printability and rheological properties of pork pastes. *Meat. Sci.* 197, 109078. <https://doi.org/10.1016/j.meatsci.2022.109078>.
- Xu, J., Fan, Y., Liu, H., Liu, Q., Zhamsharova, S., Kong, B., Chen, Q., 2023b. Improvement of rheological properties and 3D printability of pork pastes by the addition of xanthan gum. *LWT* 173. <https://doi.org/10.1016/j.lwt.2022.114325>.
- Yi, L., Lakemond, C.M., Sagis, L.M., Eisner-Schadler, V., van Huis, A., van Boekel, M.A., 2013. Extraction and characterisation of protein fractions from five insect species. *Food Chem.* 141 (4), 3341–3348. <https://doi.org/10.1016/j.foodchem.2013.05.115>.
- Yu, W., Wang, Z., Pan, Y., Jiang, P., Pan, J., Yu, C., Dong, X., 2022. Effect of κ-carrageenan on quality improvement of 3D printed Hypophthalmichthys molitrix-sea cucumber compound surimi product. *LWT* 154. <https://doi.org/10.1016/j.lwt.2021.112279>.
- Yu, X., Wang, Y., Zhao, W., Li, S., Pan, J., Prakash, S., Dong, X., 2023. Hydrophilic colloids (Konjac gum/Xanthan gum) in 3D printing of transitional food from fish paste. *Food Hydrocoll.* 137. <https://doi.org/10.1016/j.foodhyd.2022.108333>.
- Zeng, X., Chen, H., Chen, L., Zheng, B., 2021. Insights into the relationship between structure and rheological properties of starch gels in hot-extrusion 3D printing. *Food Chem.* 342, 128362. <https://doi.org/10.1016/j.foodchem.2020.128362>.
- Zhang, C., Liu, H., Xia, X., Sun, F., Kong, B., 2021. Effect of ultrasound-assisted immersion thawing on emulsifying and gelling properties of chicken myofibrillar protein. *LWT* 142. <https://doi.org/10.1016/j.lwt.2021.111016>.
- Zhang, F., Cao, C., Kong, B., Sun, F., Shen, X., Yao, X., Liu, Q., 2022. Pre-dried mealworm larvae flour could partially replace lean meat in frankfurters: effect of pre-drying methods and replacement ratios. *Meat. Sci.* 188. <https://doi.org/10.1016/j.meatsci.2022.108802>.
- Zhao, X., Vazquez-Gutierrez, J.L., Johansson, D.P., Landberg, R., Langton, M., 2016. Yellow mealworm protein for food purposes - extraction and functional properties. *PLoS One* 11 (2), e0147791. <https://doi.org/10.1371/journal.pone.0147791>.
- Zhao, Y., Li, Y., Liu, Q., Chen, Q., Sun, F., Kong, B., 2024. Investigating the rheological properties and 3D printability of tomato-starch paste with different levels of xanthan gum. *Int. J. Biol. Macromol.* 257 (Pt 1), 128430. <https://doi.org/10.1016/j.ijbiomac.2023.128430>.
- Zhao, Z., Wang, Q., Yan, B., Gao, W., Jiao, X., Huang, J., Zhao, J., Zhang, H., Chen, W., Fan, D., 2021. Synergistic effect of microwave 3D print and transglutaminase on the self-gelation of surimi during printing. *Innov. Food Sci. Emerg. Technol.* 67. <https://doi.org/10.1016/j.ifset.2020.102546>.
- Zielinska, E., Karaś, M., Baraniak, B., 2018. Comparison of functional properties of edible insects and protein preparations thereof. *LWT* 91, 168–174. <https://doi.org/10.1016/j.lwt.2018.01.058>.